

Time-Dependent Analysis of Multinucleon Transfer Reactions with Heavy Nuclei

V.V. Samarin^{1,2}

¹Joint Institute for Nuclear Research, 141980 Dubna, Russia

²Dubna State University, 141982 Dubna, Russia

Abstract. Numerical solution of the time-dependent Schrödinger equation (TDSE) is used for studying neutron and proton rearrangement and transfer processes in low-energy nucleus-nucleus collisions. The evolution of the wave functions for outer neutrons of ^{96}Zr in fusion reaction $^{40}\text{Ca} + ^{96}\text{Zr}$ and for all nucleons in reaction $^{40}\text{Ca} + ^{124}\text{Sn}$ is determined. The results of calculations of transfer cross sections are in satisfactory agreement with experimental data for reaction $^{40}\text{Ca} + ^{124}\text{Sn}$.

1 Introduction

Inelastic grazing collisions of atomic nuclei are accompanied by nucleon transfer and the deformation of the nuclear surface. The relative motion of heavy nuclei may be analyzed based on of classical mechanics by employing the concepts of the trajectory and scattering angle which depend on the impact parameter. A quantum-mechanical treatment should be applied in dealing with intrinsic degrees of freedom, such as single-particle states, low-lying (quadrupole, octupole, etc.) vibrations of nuclear surfaces, and high-lying oscillations (giant resonances). In those cases, the minimum distance R_{\min} between the centers of colliding nuclei may serve as a characteristic parameter. At rather large R_{\min} , the probabilities for nucleon transfer and collective excitations are low, which allow one to employ approximate methods including the perturbation theory, linear terms of power-series expansions, and empirical models. Touching and a partial intersection of nuclear surfaces entail deep-inelastic reactions and multinucleon transfer. In case of substantial changes in nucleon wave functions prevent the application of the perturbation theory, whereas the approach based on the time-dependent Schrödinger equation (TDSE) [1, 2] provides the possibility of theoretical description of the processes. At small impact parameters, a projectile nucleus may be captured by a target nucleus after overcoming the Coulomb barrier, and after that incomplete or complete fusion are possible. The rearrangement of outer nucleons takes place at the first stages of transfer and fusion reaction at small distances between nuclear surfaces. In the present study, the time-dependent approach is applied to individual nucleons of colliding nuclei.

2 Neutron Rearrangement at the First Stage of the Fusion in Reaction $^{40}\text{Ca} + ^{96}\text{Zr}$

At small impact parameters a projectile nucleus is captured by a target nucleus after overcoming the Coulomb barrier. In the model with the classical trajectories of colliding nuclei we may study the rearrangement of their outer neutrons before overcoming the Coulomb barrier. In general case, tunneling through Coulomb barrier may be taken into account in the coupled channel method [3]. In the independent-nucleon model, the initial spinor two-component wave functions having the projection m_j of the total angular momentum onto the z axis have the form

$$\psi_{n,l,j,m_j} = \chi_{n,l,j}(r)\Omega_{j,l,m_j}(\theta, \varphi), \quad (1)$$

where the angular parts Ω_{j,l,m_j} are the spherical spinors, $l = 0, 1, \dots, j = l \pm 1/2$, $m_j = -j, -j + 1, \dots, j$. The radial wave functions $\chi_{n,l,j}(r)$ are determined numerically for a mean field in the Woods–Saxon form. The parameters of the mean field were determined by fitting the theoretical values of the root-mean-square charge radius and the proton and neutron separation energies to their experimental counterparts (see, for example, [4]). At the approaching reaction stage the outer (valence) neutron wave function, localized initially in one of the nuclei, may spread into the volume of the other nucleus (see Figure 1a) already before the colliding nuclei have overcome the Coulomb barrier [5]. The analysis of this process was made using two-center wave functions of outer neutrons in the dinuclear system. The probability densities in the Figures 1b,c demonstrate that these wave functions with small absolute values of the total-angular-momentum projection onto the nucleusnucleus axis $|m_j| = 1/2$ and

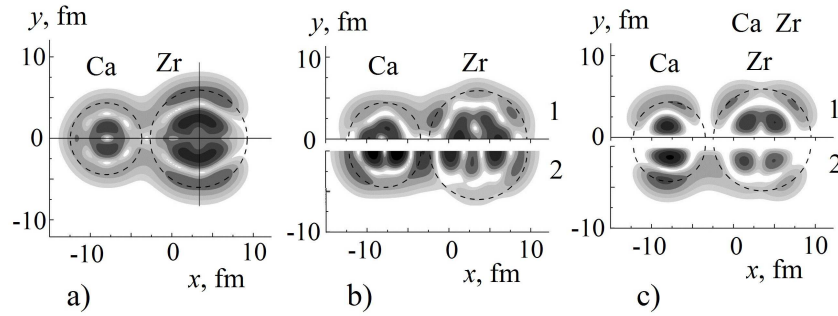


Figure 1. a) Probability density for neutrons of the $2d_{5/2}^6$ outer shell in the ^{96}Zr nucleus near the turning point in a central collision with a ^{40}Ca nucleus at $E_{c.m.} = 98$ MeV; b, c) probability densities for the two-center (molecular) states corresponding to the $2d_{5/2}$ state of the ^{96}Zr nucleus (upper part 1) and the $2p_{3/2}$ state of the ^{40}Ca nucleus (lower part 2) for the following absolute values of the total-angular-momentum projection onto the nucleusnucleus axis (x axis): $|m_j| = 1/2$ (b) and $|m_j| = 3/2$ (c).

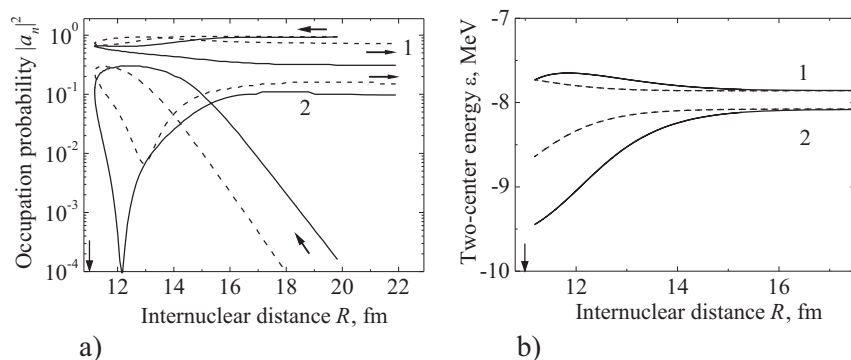


Figure 2. The occupation probabilities (a) and energies (b) for the two-center (molecular) states that correspond to the $2d_{5/2}$ state of the ^{96}Zr nucleus (curves 1) and $2p_{3/2}$ state of the ^{40}Ca nucleus (curves 2) for the absolute values $|m_j| = 1/2$ (solid curves) and $|m_j| = 3/2$ (dashed curves) of the total-angular-momentum projection onto the nucleus-nucleus axis in the head-on collision $^{40}\text{Ca} + ^{96}\text{Zr}$ at $E_{c.m.} = 98$ MeV; arrows indicate the distance of the top of the Coulomb barrier.

$|m_j| = 3/2$ are overlapping strongly for two-center (molecular) states corresponding to one-center states $2d_{5/2}$ and $2p_{3/2}$ of separate nuclei ^{96}Zr and ^{40}Ca , respectively. It leads to large probability of transition of neutrons from the first state to the second. The typical graphs of the occupation probability $|a_n(t)|^2$ of these states as a function of time are given in Figure 2a. In the vicinity of the turning point near the top of the Coulomb barrier, the occupation probability for a two-center state corresponding to one-center state $2p_{3/2}$ of Ca nucleus proves to be rather high (more than 0.1). The energies depending on internuclear distance R of paired neutrons in molecular states with $|m_j| = 1/2$ and $|m_j| = 3/2$ in the $^{40}\text{Ca} + ^{96}\text{Zr}$ system are displayed in Figure 2b. The energies of states with large angular-momentum projections onto the axis between the centers of colliding nuclei, $|m_j| \geq 3/2$, undergo virtually no changes up to the Coulomb barrier whose top is at $R_B = 11$ fm. The distance dependent energy yield $Q(R)$ for transition of two paired neutrons with $|m_j| = 1/2$ and with $|m_j| = 3/2$ from upper molecular levels to nearest lower molecular levels respectively equal to

$$Q_{2d-2p,1/2}(R) = 2[\varepsilon_{2p,1/2}(R) - \varepsilon_{2d}(\infty)], \quad (2)$$

$$Q_{2d-2p,3/2}(R) = 2[\varepsilon_{2p,3/2}(R) - \varepsilon_{2d}(\infty)]. \quad (3)$$

Some distribution on $Q < Q_{\max}$, $Q_{\max} > 0$ will take place as a result of transition of neutrons from molecular level $2d_{5/2}$ of the ^{96}Zr to lower and upper molecular levels near top of the barrier. This process may proceed with the energy gain which, in turn, may lead to a gain in the kinetic energy of relative motion (energy lift) [6, 7]. Thus, neutron rearrangement with positive Q values may significantly influence the sub-barrier fusion dynamics, leading a

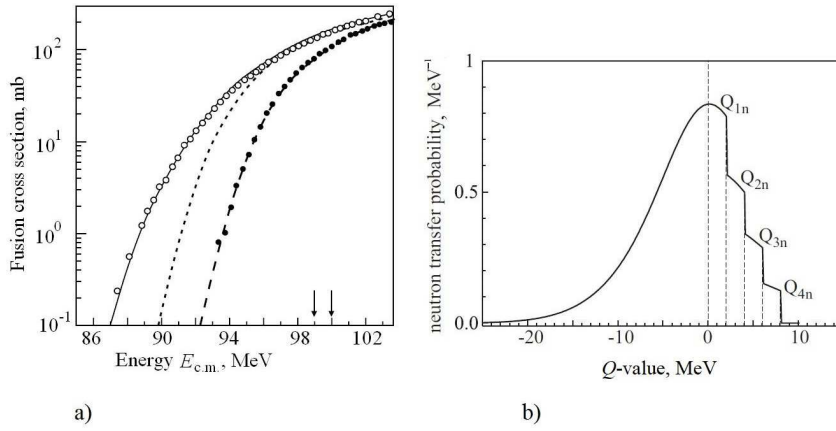


Figure 3. a) Fusion cross sections for reactions $^{40}\text{Ca}+^{90}\text{Zr}$ (filled circles) and $^{40}\text{Ca}+^{96}\text{Zr}$ (empty circles) [7, 8]. Dashed curve is the coupled channel (CC) calculation for the $^{40}\text{Ca}+^{90}\text{Zr}$ fusion reaction. Dotted curve is the CC calculations for the $^{40}\text{Ca}+^{96}\text{Zr}$ fusion reaction, whereas the solid curve is the result of calculations for the same reaction in ECC and QCC+ENR models; arrows indicate the Coulomb barrier heights. b) The typical behavior of distribution on Q -values for neutron rearrangement. The Q_{xn} values are assumed to be equal to $2x$ MeV [6].

substantial increase of the barrier penetration probability (see Figure 3a). Thus, the TDSE approach for outer neutrons of colliding nuclei provides the microscopic validation of empirical coupled-channel model (ECC [7]) and quantum coupled-channel+empirical neutron rearrangement model (QCC+ENR [6]) of fusion taking into account neutron rearrangement. In both models, gaussian-like distribution on Q -values was proposed (see Figure 3b). The parameters of this distribution depend on Q_{xn} -values and probabilities for transfer of x neutron from the ground state to the ground state of nuclei in reactions.

3 Multinucleon Transfer in Reaction $^{40}\text{Ca} + ^{124}\text{Sn}$

Touching and partial intersection of the nuclear surfaces entail deep-inelastic reactions and multinucleon transfer. TDSE approach was used for description of neutron and proton transfer in reaction $^{40}\text{Ca} + ^{124}\text{Sn}$ at energy above the Coulomb barrier. Several upper proton and neutron levels of the ^{40}Ca and ^{124}Sn nuclei are shown in Figure 4.

Six proton and neutron shells are filled in the ^{40}Ca nucleus, the $1d_{3/2}$ level being the uppermost fully filled state. In the ^{124}Sn nucleus 11 proton and 16 neutron shells are filled. The wave functions (1) were used for all neutron shells of both nuclei as the initial condition. For protons wave functions, a long-range character of the Coulomb interaction and the polarization effects were taken into account approximately. The Coulomb interaction of every proton with another

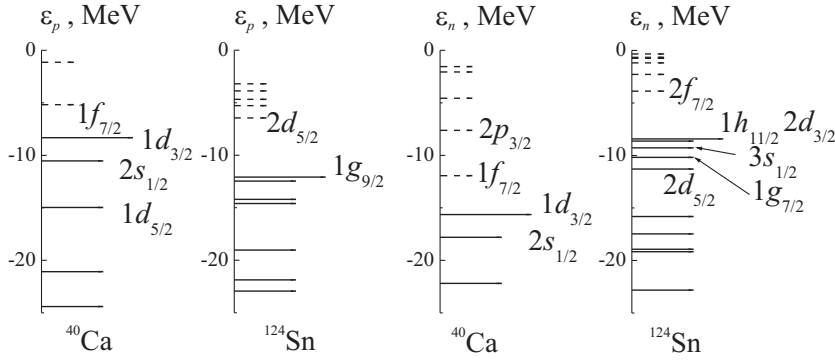


Figure 4. Proton (ε_p) and neutron (ε_n) shell-model levels of the ^{40}Ca projectile and ^{124}Sn target nuclei. The longest and the dashed segments represent respectively the Fermi levels and the unoccupied levels.

nucleus was switched on slowly (adiabatically) at finite internuclear distance. Examples of the probability density for the outer protons of the ^{40}Ca nucleus from the $1d_{3/2}$ and $2s_{1/2}$ initial states, and for the outer neutrons of the ^{124}Sn nucleus from the $2d_{3/2}$ and $3s_{1/2}$ initial states, at the distance of the closest approach of the ^{40}Ca and ^{124}Sn nuclei are given in Figure 5.

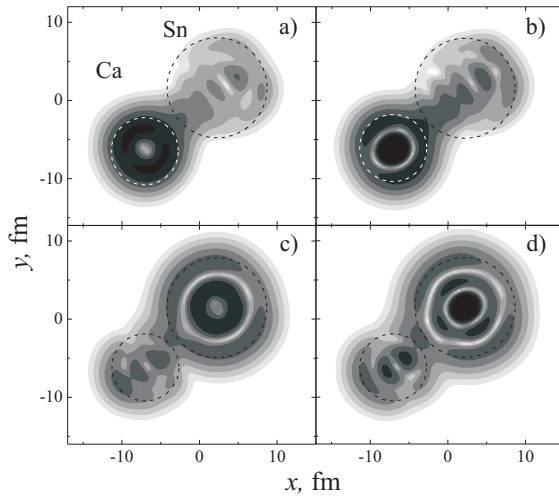


Figure 5. Probability densities at the distance of the closest approach of ^{40}Ca and ^{124}Sn nuclei for the protons of the ^{40}Ca nucleus from (a) $1d_{3/2}$ and (b) $2s_{1/2}$ initial states and for the neutrons of the ^{124}Sn nucleus from (c) $2d_{3/2}$ and (d) $3s_{1/2}$ initial states; $E_{c.m.} = 128$ MeV, the impact parameter is $b = 4$ fm. The distance between the centers of the nuclei is 12 fm, and the radii of the circles are equal to the radii of the nuclei.

The structure of the maxima and minima of the probability density clearly shows that the outer protons of the ^{40}Ca nucleus, after transfer to the ^{124}Sn nucleus, populate the free $2d_{5/2}$ state with largest probability. This is facilitated by a relatively low energy of proton separation from the ^{40}Ca nucleus (8.3 MeV [4]) and a moderately small difference between the energies of the $1d_{3/2}$, $2s_{1/2}$, and $1d_{5/2}$ initial levels in the ^{40}Ca nucleus and the $2d_{5/2}$ final level in the ^{124}Sn nucleus. Also, the absence of a centrifugal barrier favors transitions from the $2s_{1/2}$ initial state. A similar situation prevails in the case of the transition of the outer neutrons of the ^{124}Sn nucleus from the $3s_{1/2}$, $2d_{3/2}$, $2d_{5/2}$, $1g_{7/2}$, and $1h_{11/2}$ states to the $2p_{3/2}$ state of the ^{40}Ca nucleus. A large difference between the energies of the initial and final levels hampers the inverse transitions of protons from the ^{124}Sn nucleus to the free levels of the ^{40}Ca nucleus and neutrons of the ^{40}Ca nucleus to the free levels of the ^{124}Sn nucleus. An example of the evolution of the probability density for all nucleons in a $^{40}\text{Ca}+^{124}\text{Sn}$ central nucleus-nucleus collision at $E_{c.m.} = 128$ MeV is given in Figure 6.

The probabilities for the transitions of one nucleon to free levels of the other nucleus can be found by the approximate formula proposed in [9]

$$p(b, E) = \lim_{t \rightarrow \infty} \sum_k |a_k(t)|^2 \quad (4)$$

where a_k are the coefficients in the expansion of the time-dependent wave function in terms of the wave functions for single-particle states. For the three upper occupied proton levels of the ^{40}Ca nucleus, the probabilities of proton transfer

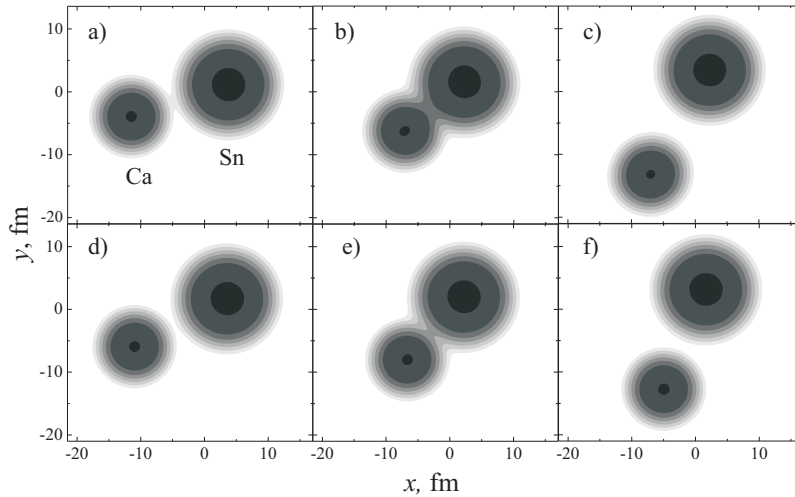


Figure 6. Evolution of the probability density for all nucleons of ^{40}Ca and ^{124}Sn nuclei at $E_{c.m.} = 128$ MeV and the impact parameter $b = 4$ fm (a, b, c) and $b = 6$ fm (d, e, f). The order of panels, (a, b, c) and (d, e, f), corresponds to the course of time.

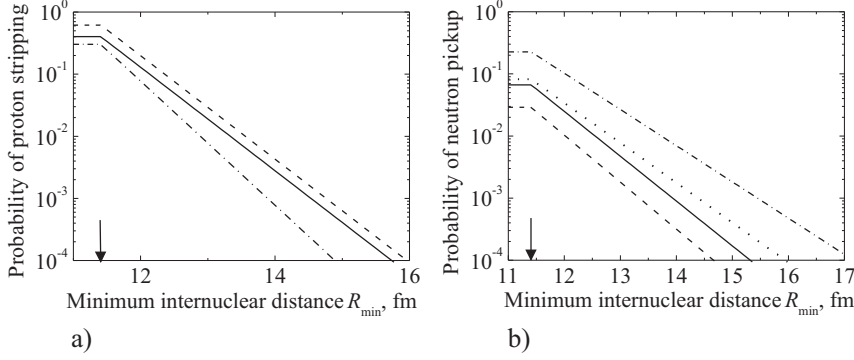


Figure 7. Proton stripping and neutron pickup in the $^{40}\text{Ca} + ^{124}\text{Sn}$ collision with the center-of-mass energy $E_{c.m.} = 128$ MeV and the minimum distance R_{\min} between the centers of the nuclei: a) probability p of the proton transfer to the ^{124}Sn nucleus from the initial $1d_{3/2}$ (solid line), $2s_{1/2}$ (dashed line), and $1d_{5/2}$ (dot-dashed line) levels of the ^{40}Ca nucleus; b) probability p of the neutron transfer to the ^{40}Ca nucleus from the initial $1h_{11/2}$ (solid line), $3s_{1/2}$, and $2d_{3/2}$ (common dot-dashed line), $2d_{5/2}$ (dotted line), $1g_{7/2}$ (dashed line) levels of the ^{124}Sn ; arrows indicate the position of the Coulomb barrier.

to the free levels of the ^{124}Sn nucleus are shown in Figure 7a as a function of the minimum distance R_{\min} between the centers of the nuclei.

At distances close and above the top of the Coulomb barrier, when $R_{\min} > R_B$, $R_B = 11.4$ fm, logarithms of the calculated probabilities can be smoothed with a good accuracy by the linear dependence

$$\lg p_i(R_{\min}) \approx A_i - B_i R_{\min}. \quad (5)$$

As in [9], for energies in the vicinity of the Coulomb barrier the approximation $p = p(R_B)$ is used on the interval of $R_1 + R_2 \leq R_{\min} \leq R_B$, R_1 and R_2 are the radii of the nuclei, $R_1 + R_2 = 10.7$ fm, $R_1 + R_2 \approx R_B$. The probabilities $P(\Delta Z, R_{\min})$ for the transfer of ΔZ protons of the twelve ones in the $1d_{3/2}$, $2s_{1/2}$, and $1d_{5/2}$ shells of the ^{40}Ca nucleus are calculated by standard methods with the aid of a binomial distribution combined with addition and multiplication theorems for probabilities. The corresponding results are shown in Figure 8.

The transfer cross sections were calculated via integration over collision impact parameters

$$\sigma = 2\pi \int_{b_{\min}}^{\infty} P(b, E) b db, \quad (6)$$

here $R_{\min}(b_{\min}) = R_1 + R_2$. The results of calculation proton-stripping cross sections agree with experimental data from [10] satisfactory (see Figure 9a).

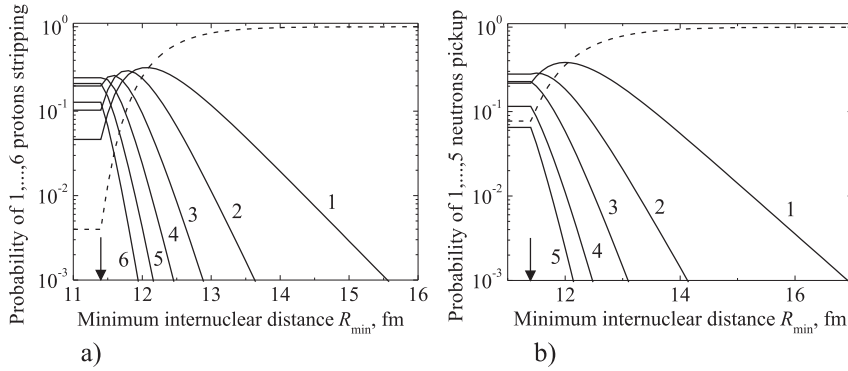


Figure 8. Proton stripping and neutron pickup in the $^{40}\text{Ca} + ^{124}\text{Sn}$ collision with the center-of-mass energy $E_{c.m.} = 128$ MeV: a) probabilities P of the stripping of $\Delta Z = 1, \dots, 6$ protons (solid lines 1, \dots , 6), the dashed line is the probability for the collision without the proton transfer ($\Delta Z = 0$), b) probabilities P of the pickup of $\Delta N = 1, \dots, 5$ neutrons (solid lines 1, \dots , 5), the dashed line is the probability for the collision without the neutrons transfer ($\Delta N = 0$); arrows indicate the position of the Coulomb barrier.

Similar results for neutron pickup by the ^{40}Ca nucleus are shown in Figure 9b. Agreement of the results of the calculations with experimental data proves to be the same as that in the proton-stripping case.

The semiclassical model developed by Winther in [11] for few-nucleon-transfer processes accompanied by a small energy dissipation was implemented within the GRAZING code [12] is widely used to calculate multinucleon-transfer cross sections. The following physical assumptions underlie the formulas used

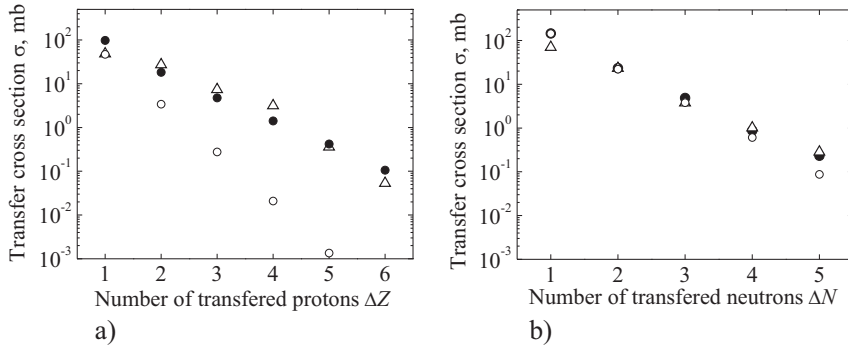


Figure 9. Proton stripping and neutron pickup in the $^{40}\text{Ca} + ^{124}\text{Sn}$ collision with $E_{c.m.} = 128$ MeV: a) cross sections for stripping of ΔZ protons without the neutron transfer, $\Delta N = 0$, b) for pickup of ΔN neutrons without the proton transfer, $\Delta Z = 0$, triangles are the experimental data [10], solid circles are the calculations using the TDSE method, empty circles are the calculations using the GRAZING code [12].

in this model for computations: single-particle transfers are independent and their probabilities are small compared to unity. The running of the GRAZING code on the NRV web server [4, 13] provides a convenient possibility for the calculation of mass and charge distributions with graphical representation of the results.

Figure 9b shows that both theoretical approaches, that of the present study and that is based on the GRAZING model, describe reasonably well the transfer of a moderately small number of neutrons (less than four) [13]. In the case of the transfer of four and five neutrons, the present time-dependent approach provides better agreement with experimental data; as for the GRAZING model, it underestimates the respective cross sections. For proton transfer (see Figure 9a), the time-dependent approach describes satisfactorily the transfer of a large number of protons, while the GRAZING model underestimates greatly the cross sections for the transfer of more than one proton.

The transfer of two protons $\Delta Z = 2$ from projectile to target changes the mean fields of both nuclei and positions of nucleon levels in the shell model. Figure 10 shows a few upper proton and neutron levels of ^{38}Ar and ^{126}Te nuclei. In the ^{38}Ar nucleus, there are six filled neutron shells with the completely filled upper level $1d_{3/2}$, and in the ^{126}Te nucleus 11 proton shells and 16 neutron shells are filled. Figure 11 shows satisfactory agreement of the results of calculation of neutron stripping and pickup cross sections for $\Delta Z = 2$ with experimental data from [10].

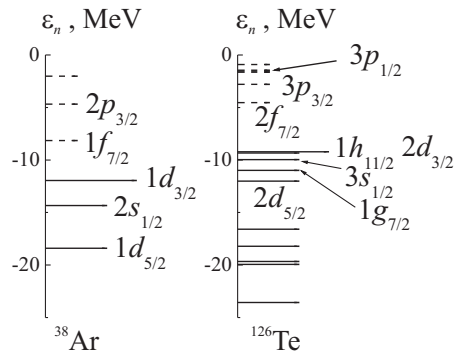


Figure 10. Neutron shell-model levels ε_n of the ^{38}Ar projectile and ^{126}Te target nuclei. The longest and the dashed segments represent respectively the Fermi levels and the unoccupied levels.

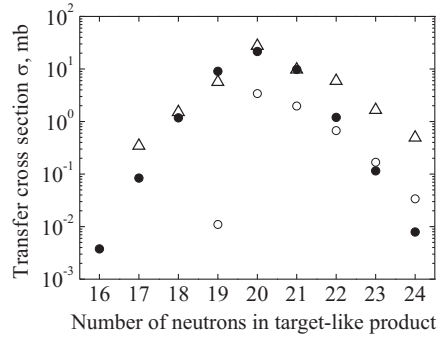


Figure 11. Neutron stripping and pickup in transfer of two protons $\Delta Z = 2$ from projectile to target in the $^{40}\text{Ca}+^{124}\text{Sn}$ collision at $E_{\text{c.m.}} = 128$ MeV, triangles are the experimental data [10], solid circles are the calculations using the TDSE method, empty circles are the calculations using the GRAZING code [12].

4 Conclusion

The numerical solution of the time-dependent Schrödinger equation is applied to analysis of dynamics of nucleon transfer and rearrangement at energies near and above the Coulomb barrier. The evolution of wave functions of all nucleons is used for the description of multi-neutron and multi-proton transfer in reaction $^{40}\text{Ca}+^{124}\text{Sn}$. The results of calculations of transfer cross sections are in satisfactory agreement with experimental data. The evolution of wave functions of outer neutrons is used for the microscopic validation of empirical neutron rearrangement (ENR) and empirical coupled-channel (ECC) models and explanation of energy dependence of fusion cross section for reaction $^{40}\text{Ca}+^{96}\text{Zr}$.

Acknowledgements

Author thanks M.A. Naumenko for aid in text processing.

References

- [1] V.V. Samarin, *Phys. Atom. Nucl.* **78** (2015) 128-141.
- [2] M.A. Naumenko and V.V. Samarin, In: *Nuclear Theory* **36** (Heron Press, Sofia, 2017) 21-30.
- [3] V.V. Samarin, *Phys. Atom. Nucl.* **78** (2015) 861-872.
- [4] V.I. Zagrebaev, A.S. Denikin, A.V. Karpov, A.P. Alekseev, M.A. Naumenko, V.A. Rachkov, V.V. Samarin, and V.V. Saiko, *NRV Web Knowledge Base on Low-Energy Nuclear Physics* [online knowledge base], URL: <http://nrw.jinr.ru/> [cited 27 September 2018].

V.V. Samarin

- [5] V.I. Zagrebaev, V.V. Samarin, and W. Greiner, *Phys. Rev. C* **75**, (2007) 035809.
- [6] A.V. Karpov, V.A. Rachkov, and V.V. Samarin, *Phys. Rev. C* **92** (2015) 064603.
- [7] V.I. Zagrebaev, *Phys. Rev. C* **67** (2003) 061601.
- [8] H. Timmers, D. Ackermann, S. Beghini, *et al.*, *Nucl. Phys. A* **633** (1998) 421-445.
- [9] M.A. Naumenko, V.V. Samarin, Yu.E. Penionzhkevich, *et al.*, *Bull. Russ. Acad. Sci.: Phys.* **80** (2016) 264-272.
- [10] L. Corradi, J.H. He, D. Ackermann, *et al.*, *Phys. Rev. C* **54** (1996) 201-205.
- [11] A. Winther, *Nucl. Phys. A* **594** (1995) 203-245.
- [12] A. Winther, GRAZING code URL: <http://personalpages.to.infn.it/nanni/grazing/> [cited 27 September 2018].
- [13] V.V. Samarin, *Bull. Russ. Acad. Sci.: Phys.* **77** (2013) 820-824.